Stability Enhancement with VSG Integration on Microgrid Systems: A Numerical Trajectory-Based Approach for Transient Analysis

Ony Asrarul Qudsi
Department of Electrical Engineering, Institut Teknologi Sepuluh Nopember Surabaya, Surabaya, Indonesia
ony@its.ac.id

Adi Soeprijanto
Department of Electrical Engineering, Institut Teknologi Sepuluh Nopember Surabaya, Surabaya, Indonesia
adisup@its.ac.id (corresponding author)

Ardyono Priyadi
Department of Electrical Engineering, Institut Teknologi Sepuluh Nopember Surabaya, Surabaya, Indonesia
ardyono@its.ac.id

Received: 19 May 2025 | Revised: 11 July 2025 and 17 July 2025 | Accepted: 19 July 2025

 DOI: https://doi.org/10.48084/etasr.12247

ABSTRACT

Stability enhancement in microgrid systems poses significant challenges, especially with high penetration of inverter-based resources. This paper proposes the integration of Virtual Synchronous Generators (VSGs) into microgrids to provide additional virtual inertia, thereby improving system stability during disturbances. A quantitative transient stability assessment based on Critical Clearing Time (CCT) is introduced to comprehensively evaluate system dynamics with VSG integration. CCT serves as a practical metric for determining the maximum allowable fault-clearing time to maintain stability, with the CCT value derived through fault trajectory analysis using the fourth-order Runge-Kutta numerical method. Resulting trajectories are classified as Stable Trajectory (ST) or Unstable Trajectory (UT) based on post-fault system response. The study is conducted on a modified IEEE 9-bus microgrid system comprising three diesel generators, with VSG integration modeled under two penetration scenarios: 11% and 29%. Simulation results show that VSG integration significantly enhances transient stability margins. However, system response is highly sensitive to fault location and duration, underscoring the need for careful system planning.

Keywords-Virtual Synchronous Generator (VSG); microgrid; Critical Clearing Time (CCT); transient stability

I. INTRODUCTION

The integration of Renewable Energy Sources (RES) remains a significant challenge in the development of microgrid systems. Recent advancements in power converter technologies have enabled RES to be integrated into microgrids [1-5], and among the inverter technologies, Grid-Forming Inverters (GFMI) have emerged as a reliable solution [6-9]. A prominent GFMI approach is the Virtual Synchronous Generator (VSG), which emulates the dynamic behavior of conventional Synchronous Generators (SGs) through virtual modeling [10, 11]. The VSG concept is particularly suitable for hybrid systems where conventional SGs coexist with inverter-based sources [4, 12-15]. Several studies have demonstrated VSGs' ability to maintain synchronism under small disturbances or gradual load variations [14-17].

Most existing studies rely on simplified system models such as the Single Machine Infinite Bus (SMIB) and evaluate transient stability using metrics like Critical Clearing Angle (CCA) or Critical Clearing Time (CCT) [18-20]. CCT is considered more relevant for practical applications, as it defines the maximum fault-clearing time that ensures the system returns to a stable condition following a disturbance [21-23], providing a more realistic evaluation of system stability during fault events.

The CCT value is determined via numerical integration of the system's nonlinear differential equations, representing

behavior before, during, and after disturbances. Fault trajectories are simulated using the fourth-order Runge-Kutta method [24]. Then, each trajectory is evaluated to verify if the system regains stability after fault clearance. If instability persists, the fault-clearing time is iteratively adjusted until the precise CCT is found. Table I presents a comparative overview of previous studies and the proposed work on transient stability enhancement in power systems.

TABLE I. COMPARISON OF RECENT STUDIES ON TRANSIENT STABILITY ENHANCEMENT STRATEGIES USING VSG IN MICROGRID SYSTEMS

Ref.	System Model	Transient Stability Strategy Enhancement	Investigation and evaluation
[2]	SMIB	GFMI	DG power sharing
[4]	Multimachine	VSG control	Pre-synchronization process
[12]	Multimachine	Parallel operation VSG and diesel SG	Low-frequency oscillation evaluation
[16]	Multimachine	Parallel operation VSG and VSC	Low-frequency oscillation evaluation
[18]	SMIB	Inertia control	Low-frequency oscillation evaluation
[19]	SMIB	VSG control	Low-frequency oscillation using CCT as a stability margin
[20]	SMIB	VSG penetration to grid	Stability under varying voltage disturbance
This paper	Multimachine	VSG penetration to grid with three diesel SGs in the system	Quantitative transient stability assessment with CCT based on numerical trajectory-based approach

This paper proposes the VSG model as a means of providing virtual inertia to microgrids, thereby improving transient stability under large disturbances. A comprehensive and quantitative approach is employed, using CCT to assess the transient stability of microgrids with integrated VSGs. To represent realistic operating conditions, transient stability analysis is performed on a modified IEEE 9-bus microgrid system comprising three diesel SGs. VSG integration is modeled under two penetration levels, 11% and 29%, reflecting scenarios of high VSG penetration [25]. The fourth-order Runge-Kutta method numerical approach was adopted to compute fault trajectories, enabling classification of system responses into stable and unstable regions and accurate determination of CCT.

II. SYSTEM MODELING

A. VSG Model

The VSG model employed is illustrated in Figure 1. In this model, V_{VSG} represents the output voltage of the VSG, while V_{PCC} denotes the voltage at the Point of Common Coupling (PCC), which serves as the interface between the VSG and the grid. The value of the V_{PCC} is obtained through the power flow iteration process. The output current of the VSG is denoted as I, with its active component contributing to the generation of active power P. The reactance X_L represents the impedance of the VSG's output filter and is calculated as the product of the filter inductance L_f and the system's angular velocity ω.

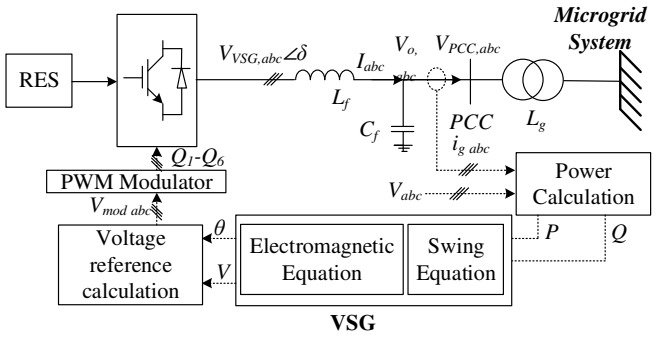

Fig. 1. Representation of the VSG model.

The reference angle of the VSG, denoted as δ_{ref}, is determined based on the voltage $V_{PCC}\angle\alpha$ as defined in (1). This reference angle is used in the inner loop control of the VSG to regulate its power output:

$$\delta_{ref} = \delta + \alpha \quad (1)$$

The dynamic behavior of the VSG is governed by the swing equation:

$$J\omega \frac{d^2\delta}{dt^2} = P_{ref} - P \quad (2)$$

$$J\omega \frac{d^2\delta}{dt^2} = P_{ref} - \frac{V_{PCC}V_{VSG}}{X_L} sin\,\delta \quad (3)$$

where J represents the virtual inertia, within the inner loop control of the VSG, and P_{ref} denotes the active power reference used in the control scheme. Based on (3), the parameters $d\delta/dt$ and δ are computed to determine the system's fault trajectory.

B. Fault Condition with VSG Integration

The transient stability of the system is evaluated based on three operating conditions: the pre-fault condition, the fault-on condition, and the post-fault condition after fault clearance with a three-phase short circuit to ground. Figure 2 illustrates the equivalent circuit representation of the system under each of these conditions.

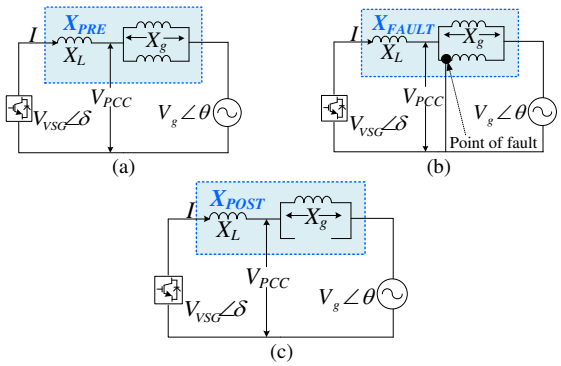

Fig. 2. System condition (a) equivalent circuit pre-fault, (b) equivalent circuit during fault, (c) equivalent circuit post-fault.

In this model, V_g represents the grid voltage, and X_g denotes the total reactance of the grid. Across the three operating

conditions, variations in X_g result in changes to the current flowing through the system. The resulting current can be calculated using (4):

$$I = \frac{V_{VSG} - V_g}{X_L - X_g} \quad (4)$$

III. PROBLEM FORMULATION

A. Center of Inertia (COI) Reference in Microgrid System with VSG

The virtual inertia provided by the VSG offers additional damping during disturbances, thereby enhancing the microgrid's ability to maintain transient stability. In the VSG interconnection scheme within the microgrid, the Center of Inertia (COI) (P_{COI}) reference is employed as a collective reference point for the rotor angle δ and angular velocity ω of all generating units in the system. This approach facilitates the observation of the relative dynamics between SGs and the VSG with respect to the overall system behavior. The P_{COI} is expressed by the following equation:

$$P_{COI} = \left(\sum_{l=1}^{n} P_{m,l} - P_{e,l}(\delta_l)\right) + \left(\sum_{k=1}^{m} P_{m,k} - P_{e,k}(\delta_k)\right) \quad (5)$$

where P_m denotes the mechanical power for SGs and the virtual mechanical power for VSGs, while P_e represents the corresponding electrical output power. Subscripts l and k refer to the l^{th} SG and the k^{th} VSG, respectively. The electrical power flows P_e are determined from the bus network considering the contributions of both SGs and VSGs as:

$$\sum_{l=1}^{n} P_{m,l} - P_{e,l}(\delta_l) = \sum_{\substack{l=1,i=1,j=1;\\ l\neq i\neq j}}^{n} (P_{m,l} - V_i^2 \frac{1}{r_{ij}}) - \sum_{i=1}^{n}\sum_{j=1,j\neq i}^{n} \left(V_i V_j \frac{1}{r_{ij}} cos\,\delta_{ij} + V_i V_j \frac{1}{l_{ij}} sin\,\delta_{ij}\right) \quad (6)$$

$$\sum_{k=1}^{m} P_k - P_{ek}(\delta_k) = \sum_{\substack{k=1,i=1,j=1;\\ k\neq i\neq j}}^{m} (P_{ki} - V_i^2 \frac{1}{r_{ij}}) - \sum_{i=1}^{m}\sum_{j=1,j\neq i}^{m} \left(V_i V_j \frac{1}{r_{ij}} cos\,\delta_{ij} + V_i V_j \frac{1}{l_{ij}} sin\,\delta_{ij}\right) \quad (7)$$

where r and l are the resistance and inductance of the transmission lines, with subscripts i and j indicating the line segment connecting bus i to bus j. Applying the COI concept, the swing equation can be reformulated as:

$$M\frac{d^2\delta}{dt^2} = \left(P_{m,l} + P_{m,k}\right) - \left(P_{e,l} + P_{e,k}\right) - \frac{M_{(l+k)}}{M_T} P_{COI} \quad (8)$$

where M is the total inertia of the microgrid and M_T is the sum of the moments of inertia from both SGs and VSGs:

$$M_T = \left(\sum_{l=1}^{n} M_l\right) + \left(\sum_{k=1}^{m} M_k\right) \quad (9)$$

B. Iterative CCT Calculation

The numerical iteration process for determining the CCT begins with initial rotor angle δ_0 and angular velocity ω_0 from the pre-fault state, continuing through to the post-fault state. These are computed as:

$$\delta_0 = \frac{1}{M_T}\left(\sum_{l=1}^{n} M_l\delta_l + \sum_{k=1}^{m} M_k\delta_k\right) \quad (10)$$

$$\omega_0 = \frac{1}{M_T}\left(\sum_{l=1}^{n} M_l\omega_l + \sum_{k=1}^{m} M_k\omega_k\right) \quad (11)$$

Equations (10) and (11) are nonlinear functions derived from the second-order differential equation:

$$x = f(x, x_0, t) \quad (12)$$

The fault trajectory is computed via the fourth-order Runge-Kutta method:

$$x_{n+1} = \begin{cases} k_1 = f(x_n, t_n)\Delta t \\ k_2 = f\left(x_n + \frac{k_1}{2}, t_n + \frac{\Delta t}{2}\right)\Delta t \\ k_3 = f\left(x_n + \frac{k_2}{2}, t_n + \frac{\Delta t}{2}\right)\Delta t \\ k_4 = f(x_n + k_3, t_n + 2)\Delta t \\ x_n + \frac{1}{6}(k_1 + 2k_2 + 2k_3 + k_4) \end{cases} \quad (13)$$

The fault trajectory is obtained during the fault period, defined over the interval [0, τ], and can be expressed by:

$$\frac{d(x)}{dt} = f(x); 0 \le t \le; x(0) = x_{PREFAULT} \quad (14)$$

$$0 \le t \le \tau \quad (15)$$

When the fault is cleared at $t = \tau$, the dynamic trajectory transitions as follows:

$$\dot{x} = f(x), \tau \le t \le \infty; f: R_N \to R_N \quad (16)$$

After the fault is cleared, the post-fault trajectory is expressed as follows:

$$x(t) = X(t; x_0), \tau \le t \le \infty; X(\cdot; x_0: R_N \to R_N) \quad (17)$$

The CCT is determined based on the post-fault trajectory when the fault is cleared at time τ, under the following condition:

$$x_0 = X_F\left(\tau; x_{pre}\right), \tau = CCT \quad (18)$$

Figure 3 illustrates the dynamic behavior of the system during and after a fault. Trajectory "1" represents the fault trajectory occurring during the disturbance. After the fault is cleared, two types of post-fault trajectories are observed. Trajectory "2" corresponds to the Stable Trajectory (ST) when the fault is cleared at δ_s, while Trajectory "3" represents the Unstable Trajectory (UT) when the fault is cleared at δ_u.

Figure 4 shows the frequency response following fault clearance at τ_s and τ_u. Using (13), the ST is obtained for τ_s, and the UT for τ_u. The time interval between ST and UT is referred to as the CCT, which can be evaluated for different fault locations.

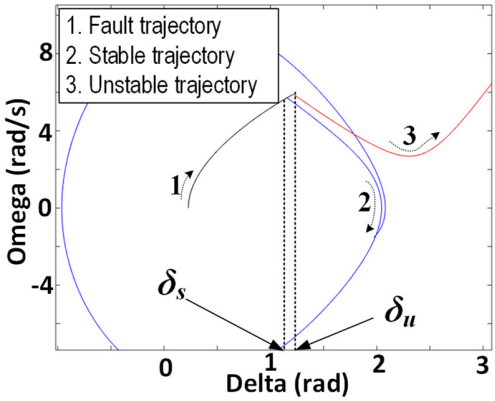

Fig. 3. Fault trajectory after fault clearance, with "1" indicating the fault trajectory.

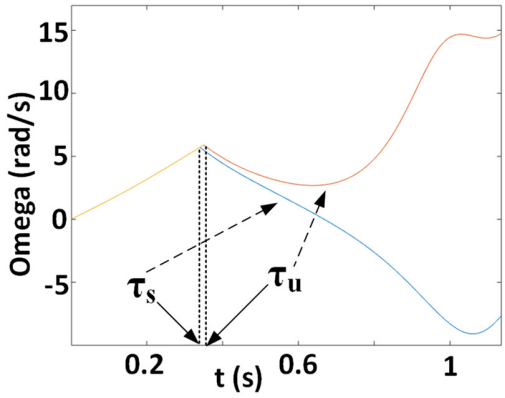

Fig. 4. Dynamic behavior of ω after fault clearance.

IV. SIMULATION RESULT AND ANALYSIS

A. Numerical Simulation for Transient Stability Analysis with VSG Integration on Microgrid System

Numerical simulations are performed on the modified IEEE 9-bus microgrid model to comprehensively evaluate transient stability under VSG integration. The system comprises three Diesel-SGs with a total capacity of 44.8 MW, supplemented by two VSG units. The microgrid configuration is shown in Figure 5. Two integration scenarios are analyzed:

- Scenario 1: VSG 1 with a capacity of 5 MW (11% penetration) is integrated.
- Scenario 2: Both VSG 1 (5 MW) and VSG 2 (8 MW) are integrated, resulting in 29% penetration.
- Fault trajectory analysis is conducted to distinguish the ST and UT after a three-phase short circuit at location "A" with different Clearing Times (CT). Figure 6 presents the angular velocity versus rotor angle curves for each SG and VSG under Scenario 2. The fault is cleared at two different CT: CT = 0.38 s and CT = 0.38 s. When the fault is cleared at CT = 0.38 s, the fault trajectory of each generator and VSG converges to the ST labeled as "1". Conversely, when the fault is cleared at CT = 0.39 s, the trajectories diverge toward the UT labeled as "2". Therefore, the ST is identified at 0.38 s, and the UT is observed at 0.39 s.

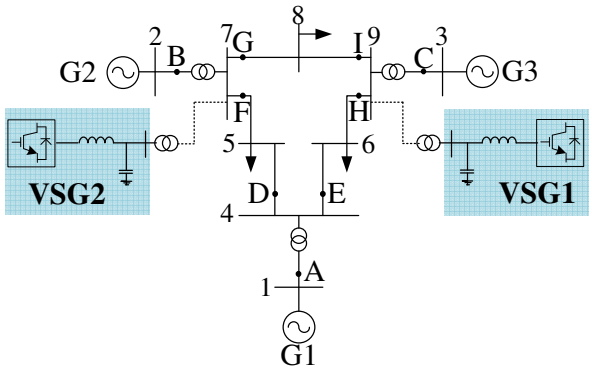

Fig. 5. Microgrid system with VSG integration.

Figure 7 illustrates the dynamic evolution of rotor angle and angular velocity for generators 1-3 and VSGs 1-2. At CT = 0.38 s, δ and ω in all units display bounded oscillations, with VSG 1 and VSG 2 exhibiting larger fluctuations but maintaining synchronism with the SGs. In contrast, at CT = 0.39 s, δ and ω in all units grow unboundedly, indicating loss of stability.

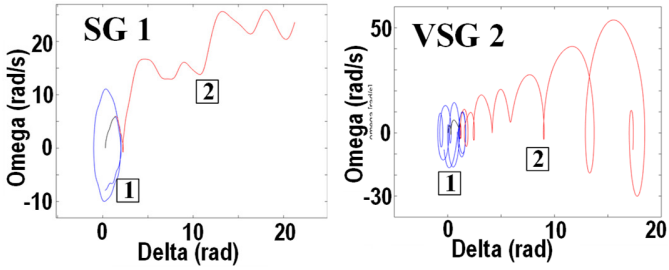

Fig. 6. Angular velocity (ω) vs angle (δ) curve of the SG 2 and the VSG 2 for fault in point "A" of IEEE 9 bus systems with scenario 2.

B. Stability Enhancement with VSG Integration on Microgrid System

Figure 8 illustrates the dynamic response of the rotor angle δ and angular velocity ω of generator 2 during a fault at location "A". As shown, generator 2 exhibits distinct changes in the behavior of δ and ω under scenario 1 and scenario 2, compared to the base case. In particular, the trajectories labeled "2" and "3" display higher values of δ_s and lower values of δ_u compared to condition "1." Similarly, ω_s in trajectories "2" and "3" is greater than in condition "1", while ω_u is lower. These findings confirm that VSG integration improves overall system stability during transient disturbances.

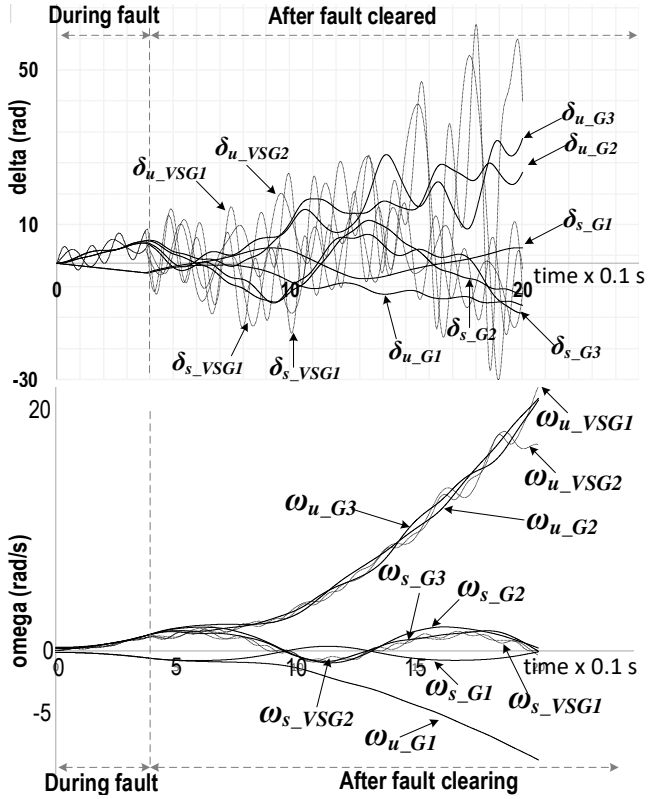

Fig. 7. Dynamic behavior of the generator 1-3 and the VSG 1-2 for fault in point "A" of IEEE 9 bus systems with scenario 2, (a) angle (δ); (b) angular velocity (ω).

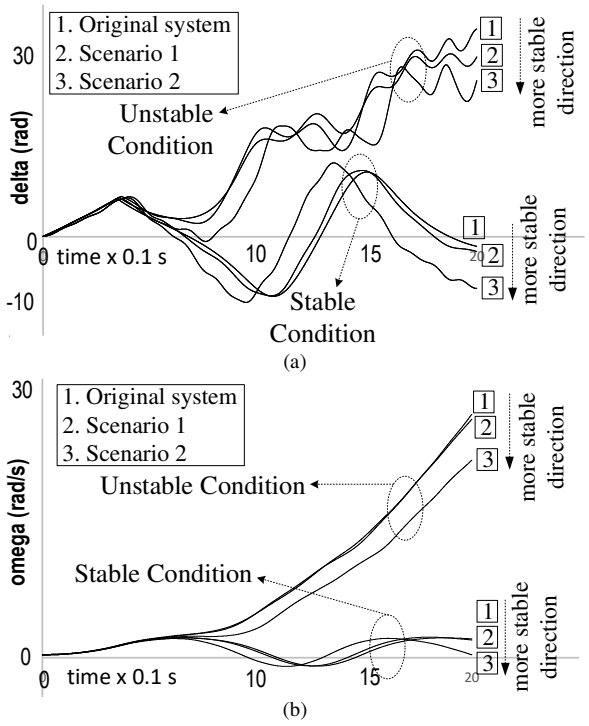

Fig. 8. The difference dynamic behavior of generator 2 for fault in point "A" of IEEE 9 bus systems, (a) Angle (δ); (b) Angular velocity (ω).

Table II presents the differences in CCT values at various fault locations in the IEEE 9-bus system under VSG integration for scenario 1 and scenario 2. Based on the results in Table II, scenario 1 integration yields increases in CCT values at fault locations "A", "C", "D", "E", and "F", with improvements ranging from 0.01 s to 0.03 s. In scenario 2, VSG integration results in CCT increases at fault locations "A", "B", "C", "D", and "E", with a broader improvement range of 0.02 s to 0.08 s.

TABLE II. CCT OF IEEE 9 BUS SYSTEMS

Fault Point	Open Line	CCT (s)		
		Without VSG	Scenario 1	Scenario 2
A	2-7	0.34 - 0.35	0.35 - 0.36	0.38 - 0.39
B	3-9	0.21 - 0.22	0.21 - 0.22	0.24 - 0.25
C	4-5	0.25 - 0.26	0.28 - 0.29	0.27 - 0.28
D	4-6	0.32 - 0.33	0.35 - 0.36	0.40 - 0.41
E	7-5	0.32 - 0.33	0.34 - 0.35	0.40 - 0.41
F	7-8	0.22 - 0.23	0.23 - 0.24	0.19 - 0.20
G	9-6	0.23 - 0.24	0.23 - 0.24	0.19 - 0.20
H	9-8	0.25 - 0.26	0.20 - 0.21	0.22 - 0.23
I	6-8	0.26 - 0.27	0.22 - 0.23	0.21 - 0.22

However, CCT reductions are observed at fault points located near the VSG integration sites. In scenario 1, CCT decreases by 0.04 s at fault locations "H" and "I". In scenario 2, reductions of 0.03 s to 0.05 s occur at locations "F", "G", "H", and "I". As shown in Figure 8, in scenario 1, VSG 1 is connected at Bus 9, which is directly linked to fault locations "H" and "I". In scenario 2, VSG 1 is connected at Bus 9 and VSG 2 at Bus 7. Since Bus 7 is directly connected to fault locations "F" and "G", and Bus 9 remains directly connected to "H" and "I", these placements explain the observed CCT reductions.

V. CONCLUSION

This study demonstrates that the integration of Virtual Synchronous Generators (VSGs) can significantly enhance the transient stability of microgrid systems. Simulation results for two VSG penetration levels (11% and 29%) show that VSG integration increases the Critical Clearing Time (CCT), thereby extending the system's stability margin. This improvement is attributed to the additional virtual inertia provided by VSGs, which enhances system resilience during transient disturbances. Nevertheless, when faults occur in close proximity to VSG connection points, the associated increase in fault current can reduce the CCT, underscoring the importance of optimal VSG placement within the microgrid. The CCT values, derived quantitatively through fault trajectory analysis using the fourth-order Runge-Kutta method, effectively characterize the system's dynamic response to faults. These results confirm that the proposed approach offers a robust framework for assessing transient stability and determining stability limits in microgrid configurations.

ACKNOWLEDGMENT

The authors gratefully acknowledge the support of the Indonesian Education Scholarship (BPI), the Centre for Higher Education Funding and Assessment (PPAPT), and the Indonesia Endowment Fund for Education (LPDP), whose contributions have been instrumental in the completion of this work.

REFERENCES

[1] S. Kakran and S. Chanana, "Smart operations of smart grids integrated with distributed generation: A review," *Renewable and Sustainable Energy Reviews*, vol. 81, pp. 524–535, Jan. 2018, https://doi.org/10.1016/j.rser.2017.07.045.

[2] M. S. Pilehvar, D. Sharma, and B. Mirafzal "Forming Interphase Microgrids in Distribution Systems Using Cooperative Inverters," *CPSS Transactions on Power Electronics and Applications*, vol. 7, no. 2, pp. 186–195, Jun. 2022, https://doi.org/10.24295/CPSSTPEA.2022.00017.

[3] S. Muchande and S. Thale, "Hierarchical Control of a Low Voltage DC Microgrid with Coordinated Power Management Strategies," *Engineering, Technology & Applied Science Research*, vol. 12, no. 1, pp. 8045–8052, Feb. 2022, https://doi.org/10.48084/etasr.4625.

[4] K. Shi, W. Song, H. Ge, P. Xu, Y. Yang, and F. Blaabjerg, "Transient Analysis of Microgrids With Parallel Synchronous Generators and Virtual Synchronous Generators," *IEEE Transactions on Energy Conversion*, vol. 35, no. 1, pp. 95–105, Mar. 2020, https://doi.org/10.1109/TEC.2019.2943888.

[5] S. Santra and M. De, "Mountain gazelle optimisation-based 3DOF-FOPID-virtual inertia controller for frequency control of low inertia microgrid," *IET Energy Systems Integration*, vol. 5, no. 4, pp. 405–417, Dec. 2023, https://doi.org/10.1049/esi2.12111.

[6] C. Cheng, S. Xie, Q. Qian, J. Lv, and J. Xu, "Observer-Based Single-Sensor Control Schemes for *LCL* -Filtered Grid-Following Inverters," *IEEE Transactions on Industrial Electronics*, vol. 70, no. 5, pp. 4887–4900, May 2023, https://doi.org/10.1109/TIE.2022.3189070.

[7] W. Du *et al.*, "Modeling of Grid-Forming and Grid-Following Inverters for Dynamic Simulation of Large-Scale Distribution Systems," *IEEE Transactions on Power Delivery*, vol. 36, no. 4, pp. 2035–2045, Aug. 2021, https://doi.org/10.1109/TPWRD.2020.3018647.

[8] Y. Li, Y. Gu, and T. C. Green, "Revisiting Grid-Forming and Grid-Following Inverters: A Duality Theory," *IEEE Transactions on Power Systems*, vol. 37, no. 6, pp. 4541–4554, Nov. 2022, https://doi.org/10.1109/TPWRS.2022.3151851.

[9] S. Chakraborty, S. Patel, and M. V. Salapaka, "Synthesis-Based Generalized Robust Framework for Grid-Following and Grid-Forming Inverters," *IEEE Transactions on Power Electronics*, vol. 38, no. 3, pp. 3163–3179, Mar. 2023, https://doi.org/10.1109/TPEL.2022.3226224.

[10] H. Wu et al., "Small-Signal Modeling and Parameters Design for Virtual Synchronous Generators," *IEEE Transactions on Industrial Electronics*, vol. 63, no. 7, pp. 4292–4303, Jul. 2016, https://doi.org/10.1109/TIE.2016.2543181.

[11] Z. Lyu, X. Gong, L. Liu, and L. Liu, "Parameters analysis and operation area calculation of VSG applied to distribution network," *CSEE Journal of Power and Energy Systems*, 2020, https://doi.org/10.17775/CSEEJPES.2019.02330.

[12] Q. Lin *et al.*, "Field Demonstration of Parallel Operation of Virtual Synchronous Controlled Grid-Forming Inverters and a Diesel Synchronous Generator in a Microgrid," *IEEE Access*, vol. 10, pp. 39095–39107, 2022, https://doi.org/10.1109/ACCESS.2022.3166953.

[13] F. Wald, Q. Tao, and G. De Carne, "Virtual Synchronous Machine Control for Asynchronous Grid Connections," *IEEE Transactions on Power Delivery*, vol. 39, no. 1, pp. 397–406, Feb. 2024, https://doi.org/10.1109/TPWRD.2023.3235149.

[14] H. Cheng, W. Huang, C. Shen, Y. Peng, Z. Shuai, and Z. J. Shen, "Transient Voltage Stability of Paralleled Synchronous and Virtual Synchronous Generators With Induction Motor Loads," *IEEE Transactions on Smart Grid*, vol. 12, no. 6, pp. 4983–4999, Nov. 2021, https://doi.org/10.1109/TSG.2021.3104655.

[15] X. Xiong, C. Wu, and F. Blaabjerg, "Effects of Virtual Resistance on Transient Stability of Virtual Synchronous Generators Under Grid Voltage Sag," *IEEE Transactions on Industrial Electronics*, vol. 69, no. 5, pp. 4754–4764, May 2022, https://doi.org/10.1109/TIE.2021.3082055.

[16] C. Shen et al., "Transient Stability and Current Injection Design of Paralleled Current-Controlled VSCs and Virtual Synchronous Generators," *IEEE Transactions on Smart Grid*, vol. 12, no. 2, pp. 1118–1134, Mar. 2021, https://doi.org/10.1109/TSG.2020.3032610.

[17] X. Xiong, C. Wu, B. Hu, D. Pan, and F. Blaabjerg, "Transient Damping Method for Improving the Synchronization Stability of Virtual Synchronous Generators," *IEEE Transactions on Power Electronics*, vol. 36, no. 7, pp. 7820–7831, Jul. 2021, https://doi.org/10.1109/TPEL.2020.3046462.

[18] D. Li, Q. Zhu, S. Lin, and X. Y. Bian, "A Self-Adaptive Inertia and Damping Combination Control of VSG to Support Frequency Stability," *IEEE Transactions on Energy Conversion*, vol. 32, no. 1, pp. 397–398, Mar. 2017, https://doi.org/10.1109/TEC.2016.2623982.

[19] P. Ge, C. Tu, F. Xiao, Q. Guo, and J. Gao, "Design-Oriented Analysis and Transient Stability Enhancement Control for a Virtual Synchronous Generator," *IEEE Transactions on Industrial Electronics*, vol. 70, no. 3, pp. 2675–2684, Mar. 2023, https://doi.org/10.1109/TIE.2022.3172761.

[20] W. Wu *et al.*, "Sequence-Impedance-Based Stability Comparison Between VSGs and Traditional Grid-Connected Inverters," *IEEE Transactions on Power Electronics*, vol. 34, no. 1, pp. 46–52, Jan. 2019, https://doi.org/10.1109/TPEL.2018.2841371.

[21] C. Mishra, R. S. Biswas, A. Pal, and V. A. Centeno, "Critical Clearing Time Sensitivity for Inequality Constrained Systems," *IEEE Transactions on Power Systems*, vol. 35, no. 2, pp. 1572–1583, Mar. 2020, https://doi.org/10.1109/TPWRS.2019.2942740.

[22] L. G. W. Roberts, A. R. Champneys, K. R. W. Bell, and M. Di Bernardo, "Analytical Approximations of Critical Clearing Time for Parametric Analysis of Power System Transient Stability," *IEEE Journal on Emerging and Selected Topics in Circuits and Systems*, vol. 5, no. 3, pp. 465–476, Sep. 2015, https://doi.org/10.1109/JETCAS.2015.2467111.

[23] N. Anwar, A. H. Hanif, H. F. Khan, and M. F. Ullah, "Transient Stability Analysis of the IEEE-9 Bus System under Multiple Contingencies," *Engineering, Technology & Applied Science Research*, vol. 10, no. 4, pp. 5925–5932, Aug. 2020, https://doi.org/10.48084/etasr.3273.

[24] N. Yorino, A. Priyadi, H. Kakui, and M. Takeshita, "A New Method for Obtaining Critical Clearing Time for Transient Stability," *IEEE Transactions on Power Systems*, vol. 25, no. 3, pp. 1620–1626, Aug. 2010, https://doi.org/10.1109/TPWRS.2009.2040003.

[25] *IEEE Application Guide for IEEE Std 1547™-2018, IEEE Standard for Interconnection and Interoperability of Distributed Energy Resources with Associated Electric Power Systems Interfaces*, IEEE Std 1547.2-2023 (Revision of IEEE Std 1547.2-2008), pp. 1–291, 2024, https://doi.org/10.1109/IEEESTD.2024.10534228.